Understanding the Growth Mechanism of α-Fe2O3 Nanoparticles through a Controlled Shape Transformation

ARTICLE *in* THE JOURNAL OF PHYSICAL CHEMISTRY C · MAY 2013

Impact Factor: 4.77 · DOI: 10.1021/jp402281a

4 AUTHORS, INCLUDING:

Ming Lin

Agency for Science, Technology and Researc…

56 PUBLICATIONS **1,387** CITATIONS

THE JOURNAL OF PHYSICAL CHEMISTRY C

Article

pubs.acs.org/JPCC

Understanding the Growth Mechanism of α-Fe_2O_3 Nanoparticles through a Controlled Shape Transformation

Ming Lin,* Hui Ru Tan, Joyce Pei Ying Tan, and Shiqiang Bai

Institute of Materials Research and Engineering, A*STAR (Agency for Science, Technology and Research), 3 Research Link, S117602, Singapore

Supporting Information

ABSTRACT: The growth mechanism of α-Fe_2O_3 nanoparticles in solution has been elucidated from a comprehensive analysis on the shape and morphology of obtained particles. It is found that the hydrothermal synthesis of α-Fe_2O_3 nanoparticles from ferric chloride precursor follows two stages: the initial nucleation of α-Fe_2O_3 nuclei and the subsequent ripening of nuclei into various shapes. The initial nucleation involves the formation of polynuclears from hydrolysis of Fe^{3+} salt precursors, followed by the growth of β-FeOOH nanowires with an akaganeite structure, and then into two-line ferrihydrite nanoparticles through a dissolution−recrystallization process. In the subsequent ripening process, we suggest that the formation of large α-Fe_2O_3 particles follows the dissolution of two-line ferrihydrite and then precipitation and oriented aggregation of α-Fe_2O_3 nuclei rather than the oriented aggregation of ferrihydrite nanoparticles followed by phase transformation. The oriented attachment of {104} facets between α-Fe_2O_3 nuclei results in the formation of oblate spheroid nanocrystals (nanoflower-like particles) either in ethanol or in the beginning stage where the particles first undergo oriented aggregation. With the addition of water, Ostwald ripening process (dissolution−reprecipitation) will play an important role to convert the assembly of nanoflowers into a 3D rhombohedral shape with well-defined edges and surfaces. The proposed mechanism in this article not only allows us to better control the synthesis of iron oxide particles with designed shapes and structures but also provides guidance for theoretical simulations on the oriented attachment process for hematite formation.

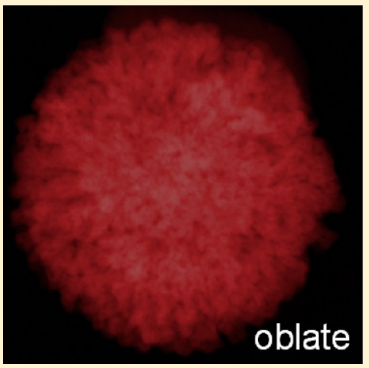

1. INTRODUCTION

Fundamental understanding of nanoparticle growth is critical for the synthesis of desired nanostructured materials with controlled composition, crystallinity, morphology, and physicochemical properties. For example, the hydrolysis of Fe^{3+} solution always yields various products, such as iron hydroxides, oxyhydroxides, oxides, and so on.[1−4] Controls on the size, shape, and crystalline structures of the iron compounds are of great importance to their distinctive applications as catalysts, adsorbents, batteries, pigments, and so on.[5−12]

Over the past few decades, intensive studies have been carried out to address the growth pathway of the iron products. Results regarding the initial nucleation of solid phases and subsequent phase evolutions have been summarized in some reviews and books.[1−3] In general, the hydrolysis of Fe^{3+} solution gives rise to the formation of intermediate iron oxyhydroxy-salt (nitrite, chloride, sulfate form) with a similar akaganeite structure prior to the formation of poorly crystallized ferrihydrite through a dissolution−reprecipitation process. Alternatively, ferrihydrite can be precipitated directly from rapid hydrolysis of Fe^{3+} in solutions. At pH >3, two-line ferrihydrite forms, whereas at lower pH and higher temperature six-line ferrihydrite precipitates (mainly hydrolyzed from $Fe(NO_3)_3$ precursor). Upon further hydrolysis, the more thermodynamically stable hematite (α-Fe_2O_3) or goethite (α-FeOOH) phases are obtained. High temperature or a neutral solution (pH ∼7) favors the formation of hematite, while the low and high pH values (pH <4, and pH >10) are preferred for the growth of goethite.[1,2] The structural transformation between various oxides and oxyhydroxides is proposed to be driven either by a dissolution-recrystallization process due to the decrease in solubility or through a topotactic transformation caused by the existence of structural continuity between hematite and ferrihydrite. In many cases, the obtained monodispersed hematite particles are found to be consisting of much smaller subcrystals, where aggregation of these smaller crystallites yields large mesocrystals, mostly with a single-crystal structure.[1−3] This process was later explained by the oriented attachment mechanism, where adjacent particles can be assembled by sharing a common crystallographic orientation to reduce the total surface energy.[13−16] This mechanism is thus considered to be a general pathway for the growth of hematite in solution and has been adopted in many publications.[17−21]

Although much is known about the formation process of hematite, details of how the hematite particles aggregate from ferrihydrite or akaganeite precursors during the oriented attachment process is still a controversy. Two possible pathways were proposed to be responsible for the formation

Received: March 6, 2013
Revised: April 15, 2013
Published: April 16, 2013

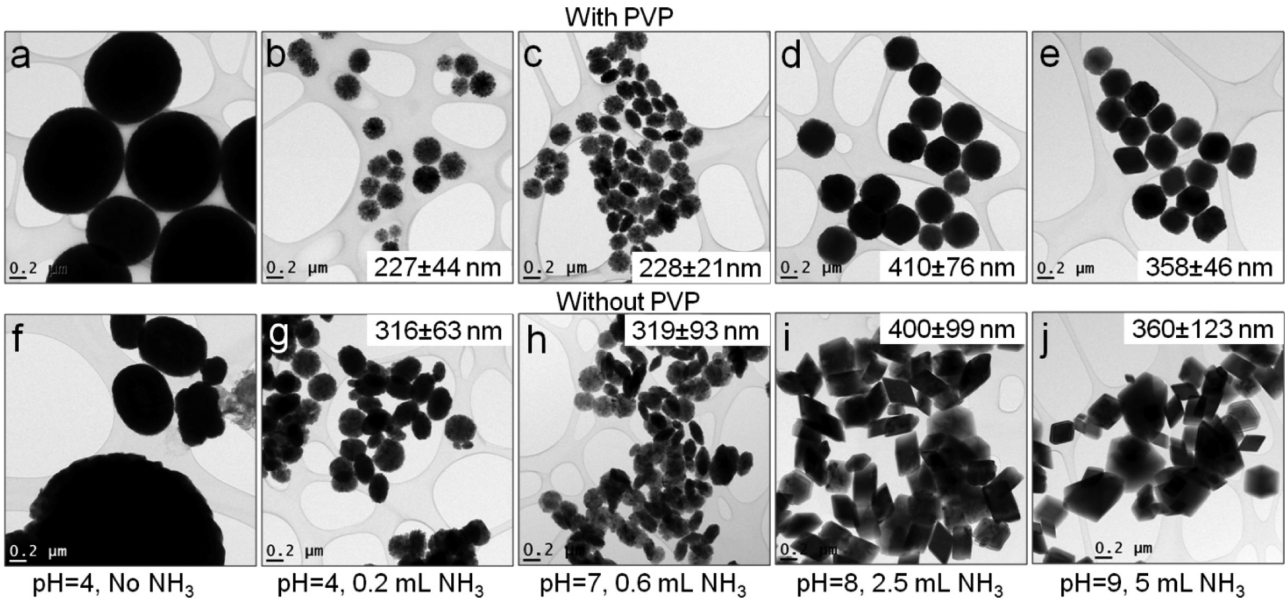

Figure 1. TEM images showing the size and shape evolution of α-Fe_2O_3 nanocrystals as a function of ammonia concentration. The average particle sizes were shown in the corresponding images.

process:[22,23] (1) oriented aggregation of the primary ferrihydrite particles followed by dehydration of ferrihydrite mesocrystals to hematite and (2) phase transformation of primary ferrihydrite particles to form hematite nanocrystals first and then self-assembly into a hematite mesocrystal. On the basis of a 16-year experiment, Schwertmann[3] concluded that the aggregation of ferrihydrite precursor was essential to induce the crystallization from ferrihydrite to hematite. Lee Penn et al.[22] further suggested that assembly of hematite particles does not occur preferentially with a specific surface plane because of the formation of equidimensional hematite particles. Alternatively, akaganeite is another precursor for the formation of hematite. It is also not established whether hematite crystallizes from dissolution of akaganeite or within aggregates of akaganeite particles by a mechanism similar to the first route of ferrihydrite to hematite. Recently, the oriented attachment between six-line ferrihydrite particles was directly observed using in situ TEM equipped with a fluid cell.[24] However, the stringent experimental conditions in the TEM-fluid cell may not lead to the formation of the same iron products as those synthesized at higher temperatures and higher pressures, thus limiting the TEM-fluid cell's application to directly track and understand the whole growth process of particles in solution.

In addition, the crystal growth can be revealed by a careful examination of the structures of the nanoparticles, where particle shape, pore structure, twin boundaries, defects, and dislocations in the crystal can reveal crucial information to the growth mechanism. Recently, with the assistance of electron tomography, we have demonstrated the 3D morphology of CeO_2 nanocrystals and unambiguously demonstrated that oriented attachment of small CeO_2 nuclei during hydrothermal process results in the formation of large and single-crystalline CeO_2 nanoparticles.[25−27] The characteristic irregular octahedral shape, occasionally with the pores orientated along ⟨110⟩ directions in the crystal, is due to oriented attachment of the exposed {111} surfaces of the CeO_2 nuclei.[26]

In this work, we have conducted a hydrothermal synthesis of α-Fe_2O_3 nanocrystals by hydrolysis of ferric chloride and investigated the growth mechanism of α-Fe_2O_3 nanoparticles from their specific shapes and morphologies. A growth mechanism has been elucidated based on comprehensive analysis of the shape and structure of the resulting particles, thus providing a reasonable description for the synthesis of α-Fe_2O_3 in solution.

2. EXPERIMENTAL SECTION

α-Fe_2O_3 nanoparticles were synthesized by a hydrothermal method. The starting solution was prepared by mixing 0.9 g of polyvinylpyrrolidone (PVP, molecular weight 30 000, final concentration 30 g/L) and 1 mmol of ferric chloride hexahydrate ($FeCl_3 \cdot 6H_2O$) in 30 mL of absolute ethanol. Different amounts of ammonium solution (12−14%, 0−5 mL) were mixed with the starting solution. The mixture was stirred for 10 min at room temperature and then transferred to a 50 mL Teflon-lined autoclave (Fisher Scientific). The autoclave was heated to 180 °C for 24 h. After reaction, the precipitate was collected and washed with ethanol and DI water. The final α-Fe_2O_3 powders were obtained by drying the precipitates at 80 °C overnight. The pH of solution was measured using litmus paper before and after the hydrothermal reaction.

The morphological and structural analyses of the obtained nanoparticles were performed on a scanning electron microscope (JEOL-6700F), an FEI Titan 80/300 scanning/transmission electron microscope (TEM) (200 kV), and an X-ray diffractometer with Cu Kα_1 radiation (λ = 1.5406 Å). To minimize the influence of washing procedures on the analysis of particle morphologies, we collected the synthesized Fe_2O_3 nanoparticles by TEM copper grids both immediately after hydrothermal reactions and after thorough wash. No obvious changes to the size and shape of particles were observed after the washing process.

A total of 77 HAADF-STEM images were collected for electron tomography over a tilt range of −76 to 76° with a 2° tilt step. Stage tilting and image acquisition were performed automatically by the FEI Xplore-3D tomography program, while tracking and refocusing of the area of interest was carried out manually to shorten the total acquisition time. Acquisition time for one 1024 × 1024 sized image was 30 s. The final tilt

dx.doi.org/10.1021/jp402281a | J. Phys. Chem. C 2013, 117, 11242−11250

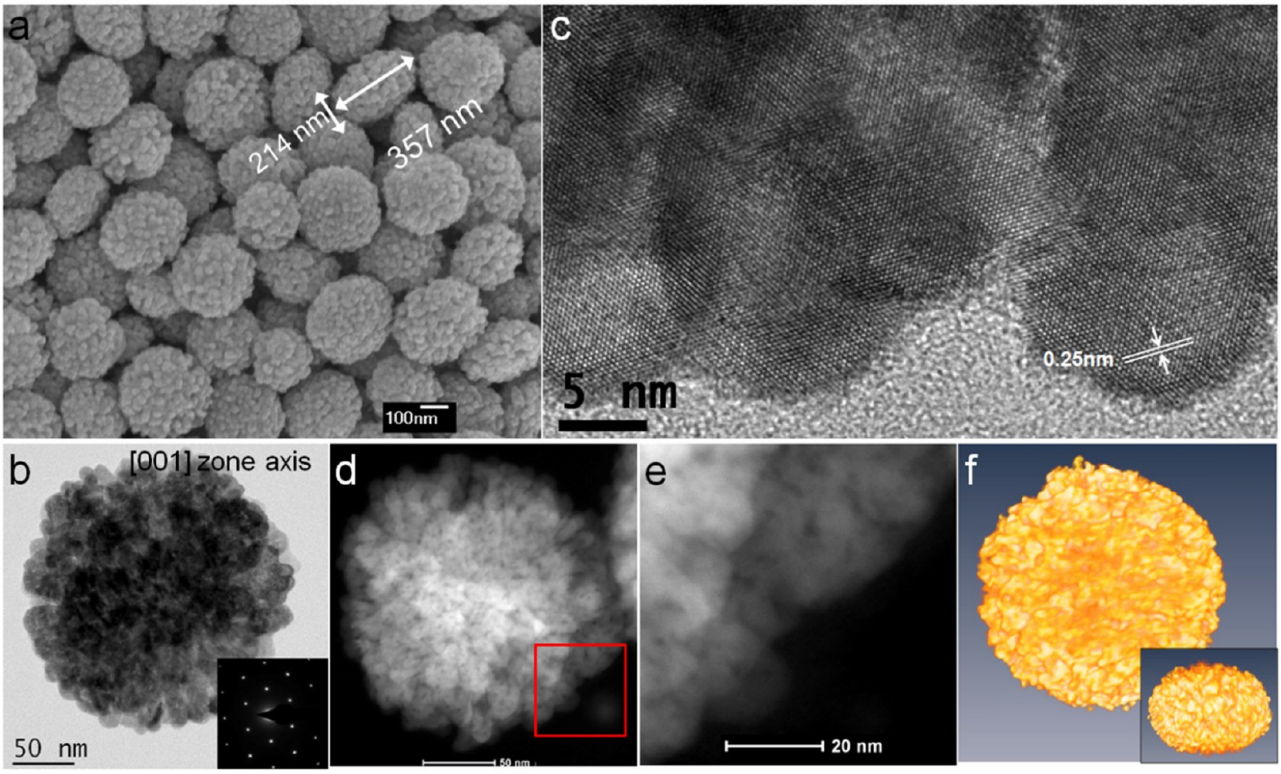

Figure 2. Structural characterization of α-Fe_2O_3 nanoflowers. (a) SEM image and (b) TEM image and corresponding diffraction pattern inset. (c) HRTEM image showing single-crystalline structures. (d,e) HAADF-STEM image. (f) Reconstructed 3D volume of a nanoflower viewing from top and side.

series was aligned using a cross-correlation method and reconstructed by the simultaneous iterative reconstruction technique (SIRT, 40 iterations) using Inspect3D, and the reconstructed 3D volume was visualized with Amira 4.1.

3. RESULTS

3.1. Controlled Synthesis of α-Fe_2O_3 Nanoparticles. In this paper, to better understand the growth process, we have maintained constant experimental temperature, time, Fe^{3+} concentration, and solution medium during synthesis. The ferric chloride was precipitated only by different amounts of ammonium solution with and without the addition of PVP. After hydrothermal synthesis, a reddish solution (color is slightly different from each other due to the various size and morphology of the obtained particles) was formed for all experiments. Figure 1 presents representative low-magnification TEM images of obtained particles as a function of NH_3 amount. All images were shown with the same magnification, and thus the size and morphology of obtained particles can be compared directly.

The particles exhibit distinctly different sizes and morphologies by changing the amount of NH_3 solution added. With the presence of NH_3 solution, microsized particles were formed with ellipsoidal shapes (Figure 1a,f). When a small amount of NH_3 was added to the solution, flower-like particles were generated and the size of particles decreased significantly to 200−400 nm, as shown in Figure 1b,c,g,h. By further increasing the amount of NH_3 solution to more than 2 mL, polyhedral particles were obtained with sharp edges and smooth surfaces (~400 nm, Figure 1d,e,i,j). XRD patterns have shown that all particles are hematite with a rhombohedral structure (α-Fe_2O_3, JCPDS no. 33-0664). The typical XRD patterns of α-Fe_2O_3 nanoflowers and nanopolyhedrons are depicted in Figure S1 in the Supporting Information.

Surfactants are often applied to restrict crystal growth in some directions through preferential absorption, thereby promoting relative growth on other crystal faces. This surface interference through absorption can result in the formation of particles with different morphologies. In this study, the presence of PVP has little influence on the size and morphology of the resulting α-Fe_2O_3 nanoparticles. The weak interaction between PVP and surface iron atoms is further confirmed by FTIR analysis (Figure S2 in the Supporting Information). Although this weak interaction cannot change the shape of the final crystals, it has two effects on the growth of α-Fe_2O_3 nanoparticles. On one hand, the agglomeration of obtained particles can be suppressed due to the adsorption of PVP.[26] Through interaction between surface hydroxyl groups on oxides and the hydroxyl groups/lactim groups of PVP,[27] the stronger steric forces between adsorbed PVP can stabilize and separate the α-Fe_2O_3 nanoparticles, leading to the formation of monodispersed crystals, as shown in Figure 1b−e. On the other hand, adsorption of PVP molecules on the surface of α-Fe_2O_3 nanocrystals also blocks the active surface sites, thus preventing the attachment of solute ions to the surface and leading to the formation of steps and defects on the surface. Therefore, the absence of PVP in solution yields agglomerated α-Fe_2O_3 nanoparticles with sharp edges and smooth surfaces.

To get insight into the growth mechanism of the α-Fe_2O_3 particles, we carefully studied two typical structures, the nanoflowers (Figure 1b) and the nanopolyhedrons (Figure 1i), by high-resolution TEM (HRTEM) and electron tomography.

dx.doi.org/10.1021/jp402281a | J. Phys. Chem. C 2013, 117, 11242−11250

3.2. Structural Characterization of α-Fe_2O_3 Nanoflowers. Two-dimensional TEM images have demonstrated α-Fe_2O_3 nanoparticles to be in the form of flower-like shapes when NH_3 solution of no more 2 mL was added in the starting solution (Figure 1b). However, rather than the symmetrical sphere that we expect to see, examination by SEM (Figure 2a) confirms that these nanoparticles have a uniform oblate spheroid 3D shape with an aspect ratio of between 1.5 and 3. According to geometry definition, an oblate spheroid is generated by rotating an ellipse around its short axis. Thus, we understand why the monodispersed α-Fe_2O_3 oblate spheroid always lies perfectly flat on the carbon membrane on TEM grids, with its long axis extending on the film and short rotating axis normal to the carbon film. SEM, TEM, and HAADF-STEM images show that the oblate α-Fe_2O_3 nanoflowers are the aggregation of small nanoparticles, with nanosized pores as small as 1 nm being observed on/in the crystal.

Selected area diffraction patterns taken from oblate α-Fe_2O_3 nanocrystals present a single crystalline structure, with the short axis of the oblate parallel to the [001] direction. By perfectly tuning the nanocrystal to its [001] zone axis, the {110} family planes with a lattice spacing of 0.25 nm can be observed in high-resolution TEM images (Figure 2c). The continuous fringes between the aggregated particles indicate that the aggregation of small particles are not random but in an ordered manner with the same crystallographic orientation. The 3D structure of nanoflower was reconstructed by electron tomography, which shows an oblate spheroid shape in Figure 2f. $x-y$ Slices taken from the center of the reconstructed volume exhibit the existence of pores not only on the surface but also embedded and sealed inside the crystal.

Because the oblate α-Fe_2O_3 nanocrystals are the aggregation of small nanoparticles, intensive ultrasonication can disintegrate the aggregated mesocrystals into small fractions due to a weak interaction between some aggregated subunits. This disintegration may be caused by dislocations or misorientations at the interface of subunits. Although diffraction patterns show a single-crystal structure of flower-like α-Fe_2O_3 nanoparticles in Figure 2b, some patterns also demonstrate slight distortion of each diffraction spot, which comprises of a major diffraction beam from mesocrystal and a few small spots surrounding it (Figure S3 in the Supporting Informaiton). This corresponds to 2 to 3° misorientation of some subcrystals to mesocrystal. The particles before and after sonication are shown in the Supporting Information (Figure S4). This confirms a high organization of most subunits in the α-Fe_2O_3 oblate spheroid together with only a few slightly misoriented subcrystals.

3.3. Structural Analysis of α-Fe_2O_3 Nanopolyhedrons. The SEM image in Figure 3 shows that each polyhedron is surrounded by six surface facets. Although smooth surfaces are observed for each particle, the HAADF-STEM image demonstrates the pores and channels in the nanoparticles (Figure 4a). SEM and TEM images only show 2D projections of 3D particles; it is difficult to identify the real crystallographic structures of the polyhedrons in 3D. Therefore, we have conducted a detailed analysis of the 3D shape and morphology of α-Fe_2O_3 nanopolyhedrons using electron tomography. Although the polyhedrons show abundant shapes in 2D SEM and TEM images, electron tomography results (measured from randomly selected 10 particles) indicate that every particle has the same rhombohedral shape, which is bounded by six identical rhombic facets. The angle between two rhombi is

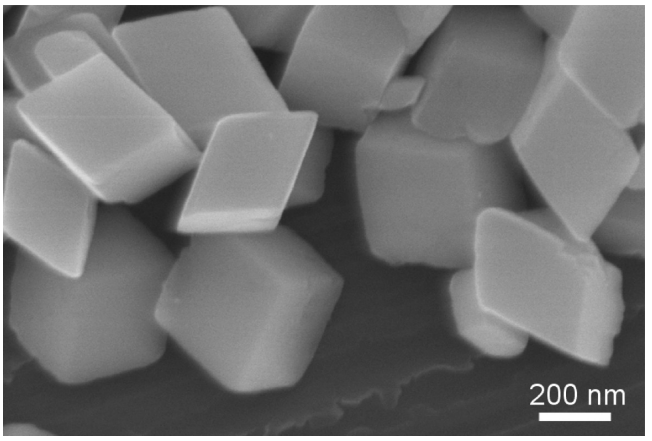

Figure 3. SEM image of α-Fe_2O_3 nanopolyhedrons.

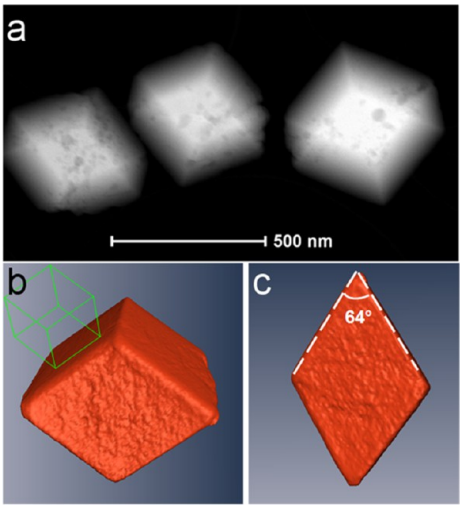

Figure 4. (a) TEM image and (b,c) reconstructed 3D volume of nanopolyhedrons showing a rhombohedral shape.

measured to be 65 ± 2°, as indicated in Figure 4c. A rough surface shown in Figure 3b,c was caused by missing wedge artifacts during tomographic reconstruction due to the limited tilt angle in TEM.

In addition to electron tomography, analysis on diffraction and high-resolution imaging by tilting nanoparticles to different zone axes was carried out to examine the crystallographic orientation of each exposed surface. It is interesting to note that the lattice fringes observed in high-resolution TEM images usually cannot be assigned to the surface facets except that the exposed surfaces are parallel to the electron beam. Therefore, the nanoparticles were tilted in TEM until the surface was parallel to the beam.

Figure 5 shows the 2D shape, corresponding diffraction pattern, and schematic drawing of rhombohedral α-Fe_2O_3 nanoparticles viewed along the [2-21], [001], [-111], and [-441] zone axes. Four different rhombohedral particles, exactly imaged at the various zone axes with double tilt holder, were selected to be presented in Figure 5 as if they were rotating around the [110] direction (the arrow shown in Figure 5b). These images have been confirmed to be representative by the sequential tilting of one particle along the [110] direction using a single tilt holder ranging from −70 to 70°. However, the diffraction patterns recorded with the single tilt holder are not

dx.doi.org/10.1021/jp402281a | J. Phys. Chem. C 2013, 117, 11242−11250

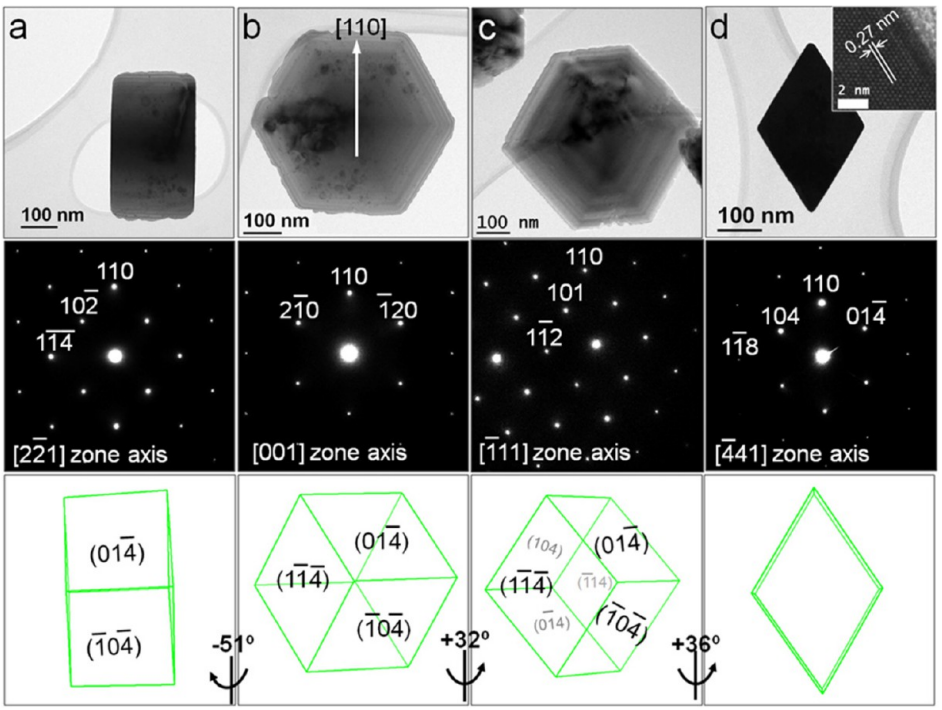

Figure 5. TEM images of rhombohedral α-Fe_2O_3 nanoparticles acquired at different zone axes and their corresponding diffraction patterns and schematic illustrations.

exactly oriented along the zone axes, while the images shown in Figure 5 can be easily interpreted.

When the particle is tilted to [-441] zone axis (Figure 5d), a perfect rhombus 2D image is observed, where four side surfaces are parallel to the electron beam. The four exposed side planes can be indexed to (01$\bar{4}$), (0$\bar{1}$4), (104) and ($\bar{1}$0$\bar{4}$) planes, respectively. The measured lattice spacing in the HRTEM image inset is 0.27 nm, corresponding to α-Fe_2O_3 (104) plane distance and extending from bulk to the surface. When the particle is tilted 36° from [-441] to [-111] zone axis, it looks like a cube with an irregular hexagonal 2D shape. Tilting the particle a further 32° to the [001] zone axis, a regular hexagonal contour is observed in Figure 5b. The strips observed in the bright-field image indicate that the edge of the particles has a wedge-like shape, where the direct and diffracted beams oscillated in a complementary way with continuous change of the wedge thickness. This further confirms the rhombohedral shape of the α-Fe_2O_3 nanocrystals. A high-resolution TEM image obtained at the [001] zone axis is shown in Figure S5 in the Supporting Information, which presents a perfect lattice-resolved structure without any defects. Further tilting 51° to [-221] zone axis, a rectangular shape is shown where the top and bottom surfaces in Figure 5d have become the two side facets in Figure 5a and can be indexed as the (1$\bar{1}$4) and ($\bar{1}$14) planes. Combining the TEM and electron tomography analysis, the α-Fe_2O_3 nanopolyhedrons can be unambiguously assigned to single-crystalline nanoparticles with a rhombohedral shape terminated with six identical {104} surfaces. The theoretical angle between {104} family planes is 64.9°, which is in good agreement with that measured by electron tomography. This conclusion also agrees very well with the morphological analysis of rhombohedral α-Fe_2O_3 crystals reported by Rodriguez et al.,[28] who synthesized rhombohedral hematite nanoparticles through forced hydrolysis of ferric chloride in acidic solution.

The rhombohedral α-Fe_2O_3 nanoparticles demonstrate various 2D contours in TEM images, such as cube, asymmetric hexagon, regular hexagon, rectangle, rhombus, and so on. The asymmetric hexagon is the typical 2D shape for the monodispersed particles on TEM grids, as shown in Figure 3a. This is because the standalone particles prefer to sit on the carbon membrane with one of its flat {104} surfaces. The [-111] zone axis is approximately perpendicular to the (-114) bottom surface with an angle of 84°. Thus, the monodispersed α-Fe_2O_3 nanoparticles demonstrate a similar 2D shape as when it is viewed along the [-111] zone axis (Figure 5c).

3.4. Growth Process of Hematite Rhombohedron As a Function of Time. To further explore the growth process of α-Fe_2O_3 rhombohedral nanoparticles, we have conducted time-dependent experiments to track the structural evolution of iron oxide particles during hydrothermal process, which are illustrated in Figure 6. Nanowires (2 to 3 μm long, 1 to 2 nm wide) and nanoparticles (1 to 2 nm) have been observed after 0.5 h of reaction at 180 °C. Because of the difficulty to monitor the reaction temperature in an autoclave, the real temperature of solution after 0.5 h reaction may not reach the desired setting (180 °C). In this case, we could capture the early nucleation states of different iron compounds. It is worth noting that quite similar results have been obtained for the fresh products before hydrothermal reaction and after 0.5 h of treatment at 180 °C.

TEM analysis indicates that the 1 to 2 nm sized particles are amorphous, where no diffraction rings can be observed in most acquired diffraction patterns. However, a careful examination of some diffraction pattern reveals a very faint ring measured at 0.25 nm, which could be probably indexed to two-line ferrihydrite (Figure S6 in the Supporting Information). It has been reported that Fe^{3+} will form $Fe(H_2O)_6^{3+}$ with the presence of water first in solution and then precipitate polynuclears through hydrolysis processes.[1] The amorphous

dx.doi.org/10.1021/jp402281a | J. Phys. Chem. C 2013, 117, 11242−11250

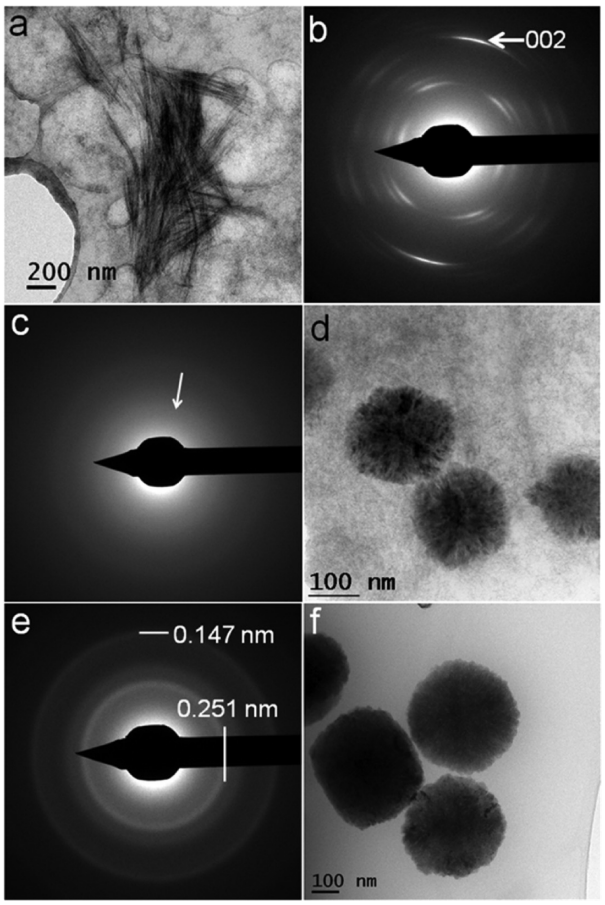

Figure 6. Shape and structural analysis of precipitates obtained at different reaction time. (a) Nanowires and nanoparticles formed at 0.5 h; (b) diffraction pattern from nanowires; (c) diffraction from nanoparticles; (d) nanoparticles and large α-Fe_2O_3 nanoflowers obtained at 3 h; (e) diffraction pattern of nanoparticles obtained at 3 h; and (f) only α-Fe_2O_3 nanoflowers obtained at 6 h. The edge becomes sharper.

particles in Figure 6a could be the polynuclears from hydrolysis of Fe^{3+} salt with water. In this context, water comes from decomposition of raw $FeCl_3{\cdot}6H_2O$ salt and trace amounts left in ethanol (<0.3%) and ammonia.

The lattice spacing of crystalline nanowires measured in the diffraction pattern is 0.334, 0.253, 0.228, 0.194, 0.178, 0.166, and 0.151 nm, respectively, corresponding to an akaganeite (β-FeOOH) structure. This structure consists of four double rows of $Fe_3(OH)_3$ octahedra, which form a square tunnel at the center. Selected area diffraction pattern taken from a bundle of aligned β-FeOOH nanowires shows strong (002) diffraction spots along the wire axis. This suggests that the β-FeOOH nanowires are elongated along the [002] direction, coinciding with the extension of the tunnel direction. EDX analysis of nanowires was performed to give the formulation of β-FeOOH nanowires at $Fe_8(OH)_8Cl_x$ ($0.1 < x < 0.2$).[2] Chloride ions are considered to stay inside the tunnels, which appear to have a structure-shaping effect to promote the transformation of amorphous polynuclear precipitate to akaganeite structures through a dissolution−reprecipitation process. In this stage, we have not observed any formation of large α-Fe_2O_3 crystals.

The solid polynuclears and intermediate β-FeOOH nanowires are not stable and further hydrolyzed to form ferrihydrite nanoparticles through the dissolution−reprecipitation process. With reaction time prolonging to 3 h, most β-FeOOH nanowires have been consumed and the diffraction pattern of nanoparticles shows two weak diffracted rings at 0.251 and 0.147 nm (Figure 6e), which can be assigned to poor crystallized two-line ferrihydrite.[13,24] The two-line ferrihydrite precipitates either from phase transformation of akaganeite nanowires or directly from the hydrolysis of polynuclears. Unfortunately we cannot differentiate the source of two-line ferrihydrite because both two-line ferrihydrite and akaganeite nanowires can be found in all reaction products from 0 to 4 h. Single-crystalline α-Fe_2O_3 nanoflowers with oblate shape are also observed after 3 h of reaction, which is the aggregation of small nanoparticles by oriented attachment process. Although the primary α-Fe_2O_3 nuclei do not show any signals in diffraction patterns taken from areas of ferrihydrite particles,

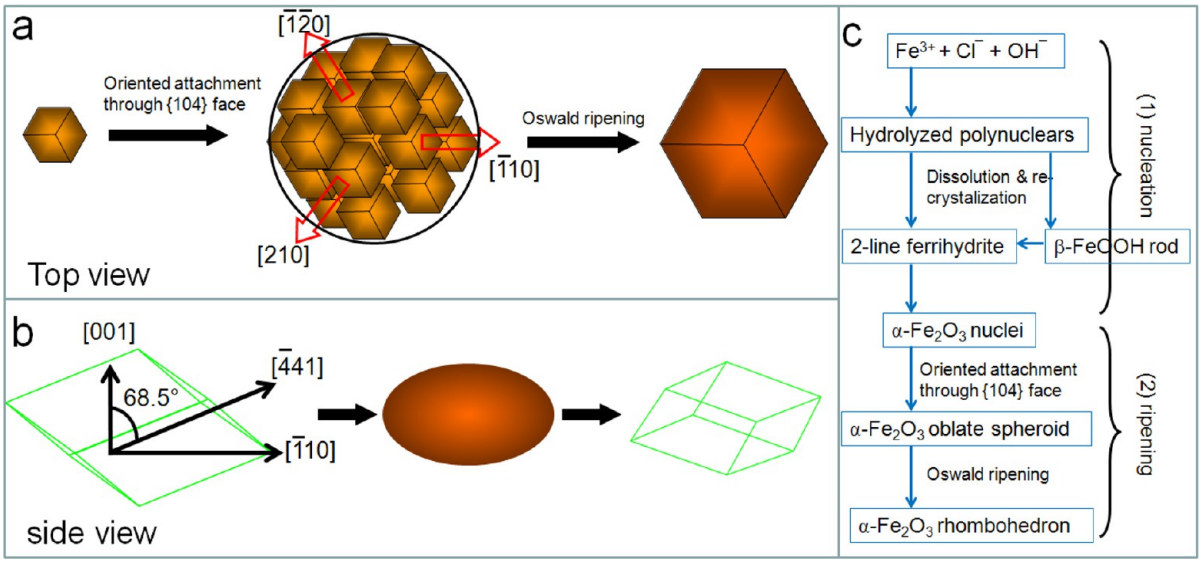

Figure 7. Schematic diagram showing the formation of α-Fe_2O_3 nanocrystals. (a) Top view of the attachment process of α-Fe_2O_3 nuclei. (b) Side view of the oriented attachment. (c) Flowchart showing the formation process of α-Fe_2O_3 nanocrystals.

dx.doi.org/10.1021/jp402281a | J. Phys. Chem. C 2013, 117, 11242−11250

examination by high-resolution TEM images reveals the presence of individual α-Fe_2O_3 nuclei among the ferrihydrite particles. These α-Fe_2O_3 nuclei can be differentiated from the ferrihydrite particles by their characteristic lattice distance shown in TEM images (Figure S6 in Supporting Information). When the reaction time extends to 6 h, faceted rhombohedral α-Fe_2O_3 crystals are obtained with the complete consumption of two-line ferrihydrite particles. This process is in good agreement with previous studies,[1−3,9,17−21] which suggests that the hydrolysis of ferric chloride leads to the formation of akaganeite and hematite.

4. DISCUSSION

On the basis of the above analysis, we propose that the hydrothermal synthesis of α-Fe_2O_3 nanoparticles from ferric chloride precursor follows two stages that have been summarized in Figure 7: (I) initial nucleation of α-Fe_2O_3 nuclei and (II) subsequent ripening of nuclei into various shapes during hydrothermal process. The nucleation process involves the formation of amorphous polynuclears, followed by nucleation into akaganeite β-FeOOH nanowires with Cl inside the channels and a subsequent phase transformation process (dissolution-recrystallization) into two-line ferrihydrite particles. Part of the two-line ferrihydrite could also be generated directly from further hydrolysis of the polynuclears. The ferrihydrite nanoparticles undergo further phase transition into more thermodynamically stable α-Fe_2O_3 nuclei. In the second stage, the α-Fe_2O_3 nuclei aggregate into single-crystalline flower-like particles through oriented attachment and then recrystallize into rhombohedral nanoparticles.

Hydrothermal synthesis is an effective method for the fabrication of monodispersed nanostructures with high purity, high crystallinity, and controlled physicochemical properties.[20] Because of the enhanced solubility at high temperature, hydrothermal reactions always result in the formation of crystals with the most thermodynamically stable structures and morphologies. The morphology of the resulting crystals can also be tuned by the addition of surfactants. The preferential adsorption of surfactants on the surface could alter the surface energies and restrict crystal growth in certain directions by attachment of ions, thereby promoting the growth of crystal into other morphologies that are stable under those reaction conditions. In this study, it is proposed that the obtained α-Fe_2O_3 rhombohedral crystals terminated with six {104} surfaces have the most stable configuration for α-Fe_2O_3 nanoparticles through the hydrolysis of ferric chloride in ethanol. The addition of PVP has little influence on the size and morphology of resulting nanoparticles. This hypothesis is further proven by the fact that this rhombohedral shape is commonly captured in TEM images in many other reports. The forced hydrolysis of ferric chloride can yield α-Fe_2O_3 rhombohedral nanoparticles, even at room temperature.[28]

We propose that the formation of large α-Fe_2O_3 particles follows the dissolution of ferrihydrite and then precipitation and oriented aggregation of α-Fe_2O_3 nuclei rather than the oriented aggregation of ferrihydrite nanoparticles followed by phase transformation. α-Fe_2O_3 nuclei, converted from ferrihydrite, are the primary precursors for the following oriented aggregation. Although these α-Fe_2O_3 nuclei are poorly crystallized (Figure S6 in the Supporting Information) without sharp edges and corners, they should have a similar rhombohedral shape with major exposed {104} planes as those stable polyhedrons. The oriented attachment of nanometer sized α-Fe_2O_3 nuclei through a lattice matched {104} face is necessary for the formation of oblate spheroid shapes. The shape and structural transformation of oxide nanocrystals has provided significant clues to the growth mechanism of oblate iron oxide in solution. Figure 7 shows the details of oriented attachment process. Viewing from [001] direction, the attachment of nuclei would extend along three identical directions, [-110], [-210], and [-1$\bar{2}$0]. The identical attachment probability of nuclei to three top and three bottom {104} surfaces gives rise to an isotropic growth within the (001) plane. However, from the side view, the attachment of nuclei on the (104) plane elongates along the [-441] direction. The angle between [-441] and [001] is 68.5°, which apparently results in an asymmetric growth rate along vertical and horizontal directions. The attachment along the [-110] direction is approximately three times faster than that along the [001] direction from a simple geometric calculation. Therefore, the isotropic growth within (001) planes and anisotropic growth within the planes perpendicular to (001) planes result in the formation of an oblate spheroid shape. This is the most reasonable mechanism that could explain the formation of oblate spheroid, instead of a regular sphere formed by isotropic aggregation in 3D directions. Moreover, we have not observed any large oriented-aggregated ferrihydrite mesocrystals during time-dependent experiments.

Because the rhombohedron has six identical α-Fe_2O_3 {104} faces, it can share one, two, or even three faces with the primary mesocrystals. Consequently, this not only significantly reduces the surface energy by removing the surface areas but also substantially decreases the stacking faults and defects by fusing two more surfaces and finding an energetically favorable position. This is also in good agreement with our findings that single crystals can be observed through high-resolution TEM analysis.

Iron oxide is an interesting material that shows a particularly high tendency toward the oriented attachment growth.[14] However, the physical driving force behind the aggregation is still unknown. Recently, direct observation of nanoparticle growth via oriented attachment in TEM suggested that electrostatic interactions between nuclei may control the aggregation process.[24] In this case, the electrostatic force between particles is caused either by the charged particles or by the charge separation on {104} polar facets. The strong interaction between nuclei leads to a fast attachment to form nanoflower-like particles in solution. The whole kinetic process may be limited by the slow conversion from ferrihydrite to α-Fe_2O_3 nuclei, partially due to the low solubility of ferrihydrite and the slow transformation through dehydration and local rearrangement.[29]

In contrast with oriented attachment process, Ostwald ripening process (dissolution−reprecipitation) can be involved in the whole reaction process. It can be achieved by the precipitation of solution ions on large crystals from the dissolution of smaller nuclei, and the dissolution and precipitation occurred at convex and concave regions of aggregated particles due to the different chemical potentials. The Fe^{3+} ions can also be from the dissolution of ferrihydrite or akaganeite particles. However, because of the low solubility of α-Fe_2O_3 crystals ($pK_{sp} \approx 10^{-43}$)[2] in absolute ethanol with trace amount of water, the Oswald ripening process is substantially prohibited. Thus, only α-Fe_2O_3 nanoflowers with oblate spheroid shape are formed through the oriented attachment of {104} facets between nuclei.

When more NH_3 solution is being added in solution, the overall increased solubility of α-Fe_2O_3 in water accelerates the dissolution−reprecipitation process, converting the assembled nanoflowers into rhombohedrons with well-defined edges and surfaces (as shown in Figure 1d,e,i,j) at 180 °C. It is interesting to note that the size and morphology of the oblate spheroid and rhombohedron are not distinctly different from each other from the top ([001] axis) and side views in Figure 7. This similarity between the two shapes makes it easy for morphological evolution from oblate spheroid to rhombohedron, even though the solubility and Oswald ripening growth rates are very low. Consistent with this explanation, we have found that rhombohedral α-Fe_2O_3 nanoparticles with smooth surfaces can be obtained in 1:1 water−ethanol mixed solution after 2 h of hydrothermal reaction, where the Ostwald ripening process was accelerated with more water in solution (Figure S7 in the Supporting Information). It is also interesting to note that due to the poor crystallization of α-Fe_2O_3 nuclei, space could be left behind during the oriented attachment process and pores are majorly formed along the edge of rhombohedral nuclei, which is shown in Figure S6c,d in the Supporting Information.

5. CONCLUSIONS

In summary, the hydrothermal synthesis of α-Fe_2O_3 nanoparticles from ferric chloride precursor includes (1) initial nucleation of α-Fe_2O_3 nuclei and (2) subsequent ripening of nuclei into various shapes. The nucleation process involves the hydrolysis of Fe^{3+} salt precursors into polynuclears and the formation of β-FeOOH nanowires with akaganeite structures, followed by the phase transformation process (dissolution−recrystallization) into two-line ferrihydrite nanoparticles and then to α-Fe_2O_3 nuclei. In the subsequent ripening process, the nuclei aggregate into a single-crystalline oblate spheroid crystals (nanoflower-like particles) through oriented attachment of {104} facets. Flower-like α-Fe_2O_3 nanocrystals can be found either in pure ethanol, where the Ostwald ripening process is suppressed by low solubility of α-Fe_2O_3, or during the beginning growth stage of crystals with higher water concentration, where the particles first undergo oriented aggregation. With the addition of water, the Ostwald ripening process (dissolution−reprecipitation) will play an important role in the reactions and convert the assembled nanoflowers into 3D rhombohedral morphology with well-defined edges and surfaces.

The size, shape, and morphological evolution clearly indicate the contribution of two ripening mechanism toward the formation of α-Fe_2O_3 nanoparticles with various shapes and morphology. The addition of PVP cannot prohibit the aggregation of nuclei through the attachment between {104} planes, but it prevents the aggregation of obtained large particles in hydrothermal reaction and gives rise to the growth of defective particles by reducing ion attachment to the particle during the Oswald ripening process.

The aggregation of α-Fe_2O_3 through oriented attachment was observed as early as in the 1980s.[2,3,30] In this paper, we first demonstrate how the initial nuclei aggregate into ordered mesocrystals structures (oblate spheroid) and recrystallize into rhombohedrons. This can be applied to explain the growth pathway of similar α-Fe_2O_3 nanocrystals reported in many other literatures. A similar phenomenon has also been observed with the other experimental conditions, such as at different temperatures, in mixed solution (ethanol−water), and change of precipitant from NH_3 to NaOH (Figure S8 in the Supporting Information). With changing experimental conditions, we found that the size, shape, and morphology of α-Fe_2O_3 nanoparticles can be fine-tuned by adjusting the competition and interplay of oriented attachment and Ostwald ripening process. Thus, we believe this is a representative and most reasonable pathway for the initial nucleation and growth of α-Fe_2O_3 in solution from ferric chloride precursor. The proposed oriented attachment of {104} facets on α-Fe_2O_3 nuclei can provide guidance to the computational simulation of hematite crystal growth. The controlled synthesis of α-Fe_2O_3 nanoparticles with defined surfaces is also critical to give the structure−property relationship for the application of hematite materials.

■ ASSOCIATED CONTENT

Ⓢ Supporting Information

XRD patterns of flower-like Fe_2O_3 nanoparticles and nanopolyhedron; TEM images of α-Fe_2O_3 oblate spherical particles before and after sonication; high-resolution TEM image of oblate spherical particle viewed along the [001] direction; selected area diffraction patterns of FeOOH nanowires and amorphous nanoparticles shown in Figure 6a in manuscript; TEM image of an incipient α-Fe_2O_3 nanorhombohedron obtained after 2 h of hydrothermal reaction with 1:1 water−ethanol solution. A video clip is also provided to show the 3D surface structure of a rhombohedral nanoparticle in Figure 4. This material is available free of charge via the Internet at http://pubs.acs.org.

■ AUTHOR INFORMATION

Corresponding Author

*E-mail: m-lin@imre.a-star.edu.sg. Tel.: 65-6874 5374. Fax: 65-6874 4778.

Notes

The authors declare no competing financial interest.

■ ACKNOWLEDGMENTS

Financial support of IMRE (IMRE/10-1C0424, IMRE/12-1P0907) is gratefully acknowledged. We thank Ms. Hanim BTE Mohamad Zain and Ms. Siti Nur'Azimah BTE Idris from Republic Polytechnic, Singapore for the assistance on the experiments.

■ REFERENCES

(1) Cornell, R. M.; Schwertmann, U. The Iron Oxides: Structure, Properties, Reactions, Occurrences and Uses; Wiley-VCH Verlag: Weinhein, Germany, 2003.

(2) Blesa, M. A.; Matijevic, E. M. Phase Transformations of Iron Oxides, Oxohydroxides, and Hydrous Oxides in Aqueous Media. *Adv. Colloid Interface Sci.* **1989**, *29*, 173−221.

(3) Schwertmann, U.; Friedl, J.; Stanjek, H. From Fe(III) Ions to Ferrihydrite and then to Hematite. *J. Colloid Interface Sci.* **1999**, *209*, 215−223.

(4) Jolivet, J.; Chaneac, C.; Tronc, E. Iron Oxide Chemistry. From Molecular Clusters to Extended Solid Networks. *Chem Commun.* **2004**, 481−487.

(5) Wan, L.; Yan, S.; Wang, X.; Li, Z.; Zou, Z. Solvothermal Synthesis of Monodisperse Iron Oxides with Various Morphologies and Their Applications in Removal of Cr(IV). *CrystEngComm* **2011**, *12*, 2727−2733.

(6) Cao, H.; Wang, G.; Zhang, L.; Liang, Y.; Zhang, S.; Zhang, X. Shape and Magnetic Properties of Single-Crystalline hematite (α-Fe_2O_3) Nanocrystals. *ChemPhysChem* **2006**, *7*, 1897−1901.

(7) Yin, J.; Yu, Z.; Gao, F.; Wang, J.; Pan, H.; Lu, Q. Low-Symmetry Iron Oxide Nanocrystals Bound by High-Index Facets. *Angew. Chem., Int. Ed.* **2010**, *49*, 6328−6332.
(8) Mou, X.; Wei, X.; Li, Y.; Shen, W. Turning Crystal-Phase and Shape of Fe_2O_3 Nanoparticles for Catalytic Applications. *CrystEngComm* **2012**, *14*, 5107−5120.
(9) Zhu, M.; Wang, Y.; Meng, D.; Qin, X.; Diao, G. Hydrothermal Synthesis of Hematite Nanoparticles and Their Electrochemical Properties. *J. Phys. Chem. C* **2012**, *116*, 16276−16285.
(10) Ma, J.; Wang, T.; Duan, X.; Lian, J.; Liu, Z.; Zheng, W. Ionothermal Synthesis of Aggregated α-Fe_2O_3 Nanoplates and Their Magnetic Properties. *Nanoscale* **2011**, *3*, 4372−4375.
(11) Zhong, Z.; Lin, M.; Ng, V.; Ng, G. H. B.; Foo, Y.; Gedanken, A. A Versatile Wet-Chemical Method for Synthesis of One-Dimensional Ferric and Other Transition Metal Oxides. *Chem. Mater.* **2006**, *18*, 6031−6036.
(12) Zhong, Z.; Highfield, J.; Lin, M.; Teo, J.; Han, Y. Insights into the Oxidation and Decomposition of CO on Au/α-Fe_2O_3 and on α-Fe_2O_3 by Coupled TG-FTIR. *Langmuir* **2008**, *24*, 8576−8582.
(13) Lee Penn, R.; Banfield, J. F. Imperfect Oriented Attachment: Dislocation Generation in Defect-Free Nanocrystals. *Science* **1998**, *281*, 969−971.
(14) Niederberger, M.; Colfen, H. Oriented Attachment and Mesocrystals: Non-classical Crystallization Mechanisms Based on Nanoparticle Assembly. *Phys. Chem. Chem. Phys.* **2006**, *8*, 3271−3287.
(15) Donnet, M.; Aimable, A.; Lemaitre, J.; Bowen, P. Contribution of Aggregation to the Growth mechanism of Seeded Calcium Carbonate Precipitation in the Presence of Polyacrylic Acid. *J. Phys. Chem. B* **2010**, *114*, 12058−12067.
(16) Zhang, H.; Banfield, J. F. Energy Calculations Predict Nanoparticle Attachment Orientations and Asymmetric Crystal Formation. *J. Phys. Chem. Lett.* **2012**, *3*, 2882−2886.
(17) Jia, B.; Gao, L. Growth of Well-Defined Cubic Hematite Single Crystals: Oriented Aggregation and Ostwald Ripening. *Cryst. Growth Des.* **2008**, *8*, 1372−1376.
(18) Chen, L.; Yang, X.; Chen, J.; Liu, J.; Wu, H.; Zhang, H.; Liang, C.; Wu, M. Continuous Shape- and Spectroscopy-Tuning of Hematite Nanocrystals. *Inorg. Chem.* **2010**, *49*, 8411−8420.
(19) Zheng, Y.; Cheng, Y.; Wang, Y.; Bao, F. Synthesis and Shape Evolution of α-Fe_2O_3 Nanophase through Two-Step Oriented Aggregation in Solvothermal System. *J. Cryst. Growth* **2005**, *284*, 221−225.
(20) Almeida, T. P.; Fay, M. W.; Zhu, Y. Q.; Brown, P. D. Hydrothermal Growth Mechanism of α-Fe_2O_3 Nanorods Derived by near in Situ Analysis. *Nanoscale* **2010**, *2*, 2390−2399.
(21) Wang, G.; Li, W.; Jia, K.; Lu, A.; Feyen, M.; Spliethoff, B.; Schuth, F. A Facile Synthesis of Shape- and Size-Controlled α-Fe_2O_3 Nanoparticles through Hydrothermal method. *Nano: Brief Rep. Rev.* **2011**, *6*, 469−479.
(22) Lee Penn, R.; Oskam, G.; Strathmann, T. J.; Searson, P. C.; Stone, A. T.; Veblen, D. R. Epitaxial Assembly in Aged Colloids. *J. Phys. Chem. B* **2001**, *105*, 2177−2182.
(23) Lee Penn, R.; Erbs, J. J.; Gulliver, D. M. Controlled Growth of alpha-FeOOH Nanorods by Exploiting-Oriented Aggregation. *J. Cryst. Growth* **2006**, *293*, 1−4.
(24) Li, D.; Nielsen, M. H.; Lee, J. R. I.; Frandsen, C.; Banfield, J. F.; Yoreo, J. J. D. Direction-Specific Interactions Control Crystal Growth by Oriented Attachment. *Science* **2012**, *336*, 1014−1018.
(25) Tan, J. P. Y.; Tan, H. R.; Boothroyd, C.; Foo, Y. L.; He, C. B.; Lin, M. Three-Dimensional Structure of CeO_2 Nanocrystals. *J. Phys. Chem. C* **2011**, *115*, 3544−3551.
(26) Tan, H. R.; Tan, J. P. Y.; Boothroyd, C.; Hansen, T. W.; Foo, Y. L.; Lin, M. Experimental Evidence for Self-Assembly of CeO_2 Particles in Solution: Formation of Single-Crystalline Porous CeO_2 Nanocrystals. *J. Phys. Chem. C* **2012**, *116*, 242−247.
(27) Lin, M.; Fu, Z. Y.; Tan, H. R.; Tan, J. P. Y.; Ng, S. C.; Teo, E. Hydrothermal Synthesis of CeO_2 Nanocrystals: Ostwald Ripening or Oriented Attachment? Cryst. *Growth Des.* **2012**, *12*, 3296−3303.
(28) Rodriguez, R. D.; Demaille, D.; Lacaze, E.; Jupille, J.; Chaneac, C.; Jolivet, J. Rhombohedral Shape of Hematite Nanocrystals Synthesized via Thermolysis of an Additive-free Ferric Chloride Solution. *J. Phys. Chem. C* **2007**, *111*, 16866−16870.
(29) Cudennec, Y.; Lecerf, A. The Transformation of Ferrihydrite into Goethite or Hematite, Revisited. *J. Solid State Chem.* **2006**, *179*, 716−722.
(30) Eisenlauer, J.; Matijevic, E. Interactions of Metal Hydrous Oxides with Chelating Agents. II. α-Fe_2O_3-low molecular and Polymeric Hydroxamic Acid Species. *J. Colloid Interface Sci.* **1980**, *75*, 199−211.